BASIC SCIENCE

Nanomedicine: Nanotechnology, Biology, and Medicine 6 (2010) 738–744

nanomedicine

www.nanomedjournal.com

Original Article

Phosphate ester hydrolysis of biologically relevant molecules by cerium oxide nanoparticles

Melissa Hirsch Kuchma, PhD[a,*], Christopher B. Komanski, BS[a], Jimmie Colon, MS[a], Andrew Teblum, BS[b], Artëm E. Masunov, PhD[b,c,d], Beatrice Alvarado, MS[a], Suresh Babu, PhD[b,e], Sudipta Seal, PhD[b,e], Justin Summy, PhD[a], Cheryl H. Baker, PhD[a,f]

[a]*Cancer Research Institute, M. D. Anderson Cancer Center Orlando, Orlando, Florida, USA*
[b]*NanoScience and Technology Center, University of Central Florida, Orlando, Florida, USA*
[c]*Department of Chemistry, University of Central Florida, Orlando, Florida, USA*
[d]*Department of Physics, University of Central Florida, Orlando, Florida, USA*
[e]*Advanced Materials Processing and Analysis Center and Mechanical Materials Aerospace Engineering, University of Central Florida, Orlando, Florida, USA*
[f]*Burnett School of Biomedical Sciences, University of Central Florida, Orlando, Florida, USA*

Received 19 October 2009; accepted 6 May 2010

Abstract

In an effort to characterize the interaction of cerium oxide nanoparticles (CNPs) in biological systems, we explored the reactivity of CNPs with the phosphate ester bonds of *p*-nitrophenylphosphate (pNPP), ATP, *o*-phospho-L-tyrosine, and DNA. The activity of the bond cleavage for pNPP at pH 7 is calculated to be 0.860 ± 0.010 nmol *p*-nitrophenol/min/μg CNPs. Interestingly, when CNPs bind to plasmid DNA, no cleavage products are detected. While cerium(IV) complexes generally exhibit the ability to break phosphorus-oxygen bonds, the reactions we report appear to be dependent on the availability of cerium(III) sites, not cerium(IV) sites. We investigated the dephosphorylation mechanism from the first principles and find the reaction proceeds through inversion of the phosphate group similar to an S_N2 mechanism. The ability of CNPs to interact with phosphate ester bonds of biologically relevant molecules has important implications for their use as potential therapeutics.

From the Clinical Editor: The ability of cerium oxide nanoparticles to interact with phosphate ester bonds of biologically relevant molecules has important implications for their use as potential therapeutics. This team of investigators explored the reactivity of these nanoparticles with the phosphate ester bonds of p-nitrophenylphosphate, ATP, o-phospho-L-tyrosine, and DNA.

Key words: Cerium oxide nanoparticle; Phosphate ester hydrolysis; Nanoceria; Phosphatase mimetic; Dephosphorylation

Most recently, cerium oxide nanoparticles (CNPs) have become an area of interest because of their potential applications to biological systems, particularly as therapeutics. CNPs have been demonstrated to act as radioprotective agents,[1,2] and as a potential therapeutic for glaucoma and blindness.[3,4] The redox chemistry of CNPs, specifically the capability to cycle between the +3 and the +4 oxidation states, may contribute to this unique reactivity in biological systems. Nonetheless, the chemistry of CNPs in biological systems is not well understood, and there are many potential interactions and reactions in which these nanoparticles can participate. Therefore, in order for CNPs to be considered as potential therapeutics, a greater understanding of their reactivity with biologically relevant molecules is required. The phosphate ester bond is ubiquitous in biological molecules, and the interaction of CNPs with DNA, RNA, phosphorylated proteins, and ATP is of particular interest.

The phosphate ester bond is crucial for regulation of protein activity, for energy transfer molecules, and for the stability of DNA and RNA. A number of transition metal and lanthanide series metal complexes are effective in hydrolysis of phosphate ester bonds.[5-8] In particular, cerium(IV) ($Ce_{(IV)}$) complexes tend to exhibit high catalytic reactivity in this reaction,[9] more so than cerium(III) ($Ce_{(III)}$) complexes. The effectiveness of these complexes can be attributed to the Lewis acidity of the metal, which

This collaboration was made possible through the support of the M. D. Anderson Cancer Center Orlando and the University of Central Florida. This project was funded in part by the National Science Foundation Grant CBET: NIRT 0708172 (to S.S.). A.M. is grateful to the National Science Foundation for financial support (NIRT project CBET-0708172) and to the Department of Energy, National Energy Research Scientific Computing Center.

*Corresponding author: Cancer Research Institute, M. D. Anderson Cancer Center Orlando, 6900 Lake Nona Blvd, Orlando, Florida 32827, USA.
E-mail address: melissa.kuchma@orlandohealth.com (M.H. Kuchma).

1549-9634/$ – see front matter © 2010 Elsevier Inc. All rights reserved.
doi:10.1016/j.nano.2010.05.004

facilitates interactions with the negatively charged phosphate moiety. These reactions occur in the presence of base[10-12] or in the presence of an intramolecular hydroxide group.[5,12] Specifically, $Ce_{(IV)}$ complexes can hydrolyze the phosphorus-oxygen bonds of DNA and RNA.[6,9,13] Dinuclear cerium complexes are also effective in DNA hydrolysis.[14] Furthermore, cerium oxide powder (1–10 μm) can dephosphorylate phosphopeptides, with the high catalytic activity attributed to the multinuclear metal complex.[15]

In this study, we investigated the chemistry of CNPs (3–5 nm) with phosphate ester bonds. We report that CNPs cleave the phosphate ester bond of pNPP, *o*-phospho-L-tyrosine, and ATP, thus acting as a phosphatase mimetic. This reaction is dependent on the availability of $Ce_{(III)}$ sites, which are present due to oxygen vacancies. However, CNPs bind plasmid DNA, and no hydrolysis products are detected. Therefore, CNPs may be able to hydrolyze ATP and phosphorylated proteins, but not DNA, in a biological system.

We also report the first principles study of the catalytic dephosphorylation mechanism of pNPP on the model dinuclear fragment of cerium hydroxide. The activation energy of dephosphorylation (22.9 kcal/mol) decreases to 16.0 kcal/mol upon the reduction of one of the $Ce_{(IV)}$ atoms to $Ce_{(III)}$ and again to 13.6 kcal/mol upon the reduction of a second $Ce_{(IV)}$ atom. We find the origin of this effect to be purely electronic, explaining the extremely slow rate of DNA hydrolysis by the steric hinderance of the reaction center.

These studies demonstrate for the first time to our knowledge that CNPs can hydrolyze phosphate ester bonds and can hydrolyze the bonds of biologically relevant molecules under physiological conditions. These findings have important implications for the use of CNPs as therapeutic agents. Further studies are under way to determine the cellular localization of CNPs in the cell.

Methods

All chemicals were obtained from Sigma-Aldrich (St. Louis, Missouri) and used without further purification unless otherwise noted. Malachite green (4-[(4-dimethylaminophenyl)-phenylmethyl]-*N*,*N*-dimethyl-aniline) in 10 mM ammonium molybdate was obtained from Millipore (Billerica, Massachusetts) as part of the PTP Assay Kit 1. Absorbance readings were taken on either a BioTek (Winooski, Vermont) ELx8081IU or Optima Fluor Star (BMG LabTech, Offenburg, Germany) spectrophotometer. DNA gels were imaged on a Gel Logic 200 Imaging System (Kodak, Rochester, New York) or on a FlashGel (Lonza, Basel, Switzerland) system.

CNP synthesis

All chemicals (Sigma-Aldrich) used in the synthesis had a purity >99%. CNPs were synthesized via a microemulsion process using sodium bis(2-ethylhexyl) sulfosuccinate as surfactant, and toluene and water as organic and inorganic phases, respectively. Sodium bis(2-ethylhexyl) sulfosuccinate was dissolved in 50 mL of toluene, and 2.5 mL of 0.1 M aqueous cerium nitrate hexahydrate was added. The mixture was stirred for 45 minutes, and 5 mL of 30% hydrogen peroxide solution was then added dropwise. After 1 hour, the reaction mixture was allowed to separate into two layers. The upper layer was toluene containing nonagglomerated ceria nanoparticles, and the lower layer was aqueous phase. CNPs were precipitated by the addition of 30% ammonia solution and washed several times with acetone and water for complete removal of the surfactant. CNPs were resuspended in deionized water at a concentration of 50 mM. Dilutions from this stock solution were used in all subsequent experiments.

Nanoparticle characterization

The synthesized CNPs were characterized using x-ray photoelectron spectroscopy (XPS) and high-resolution transmission electron microscopy (HRTEM). The ceria particles were deposited on the carbon-coated copper grid for HRTEM analysis by dip-coating method. The HRTEM images of the prepared particles were obtained with Philips (Tecnai F30; Eindhoven, The Netherlands) transmission electron microscope operating at 300 keV. The XPS data were obtained using a Perkin-Elmer (Waltham, Massachusetts) 5400 PHI ESCA (XPS) spectrometer. The base pressure during XPS analysis was 10^{-8} Torr, and Mg-K_α x-radiation (1253.6 eV) at a power of 300 W was used. The high-resolution narrow spectra were recorded with electron pass energy of 35.75 eV to achieve the maximum spectral resolution. The binding energy of the Au ($4f_{7/2}$) at 84.0 ± 0.1 eV was used to calibrate the binding energy scale of the spectrometer. Any charging shift produced by the samples was carefully removed by using a binding energy scale referred to that of 284.6 eV of C (1s) of the hydrocarbon part of the adventitious carbon line.

The size of the nanoparticles from this preparation is 3–5 nm, and they can be classified as hard nanoparticles [H-3].[16] The concentration of $Ce_{(III)}$ is calculated to be 40% due to the presence of oxygen vacancies in the lattice. As the size of the nanoparticle increases, the number of oxygen vacancies decreases, and thus, the ratio of $Ce_{(III)}$ to $Ce_{(IV)}$ decreases.[17]

Reaction of CNPs and pNPP

A 5 mg/mL solution of pNPP was prepared in deionized water. A volume of 120 μL of pNPP was added to the wells of a 96-well plate for enzyme-linked immunosorbent assay (ELISA). CNPs were added from a solution (5.0 mM) so that the final concentration in the wells ranged from 25 μM to 200 μM. The total volume in each well was adjusted to 200 μL using deionized water. Absorbance readings were taken in triplicate at 405 nm at pH 7 every minute for up to 20 minutes. ^{1}H nuclear magnetic resonance spectra were obtained on a 500-MHz Varian (Palo Alto, California) spectrometer to confirm the presence of the *p*-nitrophenol product (data not shown). For the pH studies, an apparent extinction coefficient was determined for each pH and applied to normalize the absorbance to *p*-nitrophenol at pH 7 to account for the pH dependence of the extinction coefficient of *p*-nitrophenol.[18] The concentration of CNPs used in the pH studies was 0.1 mM.

Hydrogen peroxide pretreatment of nanoparticles

CNPs were treated with 3% hydrogen peroxide. An aliquot of the cerium oxide stock solution (4.5 μL) was added to 100 μL hydrogen peroxide and vortexed. The color of the nanoparticles changed from yellow to orange, indicating a shift in oxidation state from +3 to +4. After 10 minutes the nanoparticles were centrifuged, and the supernatant was removed via aspiration. The nanoparticles were washed with 500 μL of deionized water, centrifuged, and resuspended in 50 μL of deionized water. For the experiments comparing the activity of peroxide-treated nanoparticles to untreated nanoparticles, deoinized water was added in the place of hydrogen peroxide, and all subsequent steps were followed as outlined above. The pretreated nanoparticles were used in the pNPP reaction as described above.

Free inorganic phosphate determination

The amount of inorganic phosphate liberated into solution during the phosphate ester cleavage reactions was measured using a malachite green assay. Briefly, CNPs were added to the phosphate substrate (pNPP, *o*-phospho-L-tyrosine, or ATP), and the reaction was monitored at intervals ranging from 20 minutes to 6 hours. The *o*-phospho-L-tyrosine required heating to 37°C for the reaction to proceed. Then, the mixture was centrifuged, and the supernatant was added in triplicate to a 96-well ELISA plate. A phosphate standard curve was generated using KH_2PO_4. The malachite green solution was prepared according to the kit instructions, was added to the wells, and was read at 620 nm after 15 minutes. A sample containing only the supernatant from nanoparticles (no phosphate substrate) in water was used as a negative control. The phosphate substrate plus malachite green was used as a blank.

CNPs and DNA

CNPs (in concentrations ranging from 5 mM to 37.5 mM) were incubated at 37°C for 2 hours with 5 μL murine telomerase reverse transcriptase (mTERT) DNA plasmid (80 ng/μL). After centrifugation, the supernatant was loaded onto a 1% agarose gel. DNA plasmid that was not exposed to CNPs was loaded as a control. Additional experiments were performed in which the free-phosphate concentration was monitored by the malachite green assay. In these experiments, 5 μL mTERT plasmid was incubated with CNPs (25 mM to 40 mM) for 4 hours at room temperature (23-25°C). A separate set of samples was prepared in the same way and incubated for 4 hours at 37°C.

Simulations from first principles

Gaussian 2003 Rev.D1 suite of programs[19] was used for all calculations. Program Molden was used for structure and orbital visualization.[20] The SBKJC medium-sized effective core potential and associated basis set[21] was used for Ce atoms, 6-31G basis set was used for all other atoms. The optimization was conducted at Hartree-Fock theory level with single-point energy refinement done at unrestricted Density Functional Theory level with polarized basis set 6-31G* and polarizable continuum model (PCM) to implicitly account for solvation effects (keyword SCRF = IEFPCM). Among the density functions available in Gaussian, Boese-Martin functional for Kinetics (BMK) was chosen because it was specially designed to accurately reproduce the activation energy barriers.[22] The transition state (TS) with trigonal bipyramidal configuration around the phosphorus atom was located using Synchronous Transit-Guided Quasi-Newton method (keyword Opt = QST3),[23] while the reaction pathway was established during backward and forward steepest descent from this TS (keyword IRC). The quadratic self-consistent field (SCF) convergence algorithm was used when necessary (keyword SCF = XQC). Due to multiple quasi degeneracies of the *f*-orbitals, the SCF procedure for the system containing $Ce_{(III)}$ tends to converge to one of the local minima in the orbital space, of which only the global minimum must be selected to describe the ground state of the system. To find the global minimum, we employed the following strategy.[24] The SCF procedure was converged for the system containing one less electron. The resulting orbitals were used as an initial guess for the neutral system, and the additional electron was placed on each of the available vacant orbitals of *f*-character localized on $Ce_{(IV)}$ (keyword Guess = Alter). The lowest energy SCF solution was selected as the global minimum and followed in the geometry optimizations (keyword Guess = NoExtra).

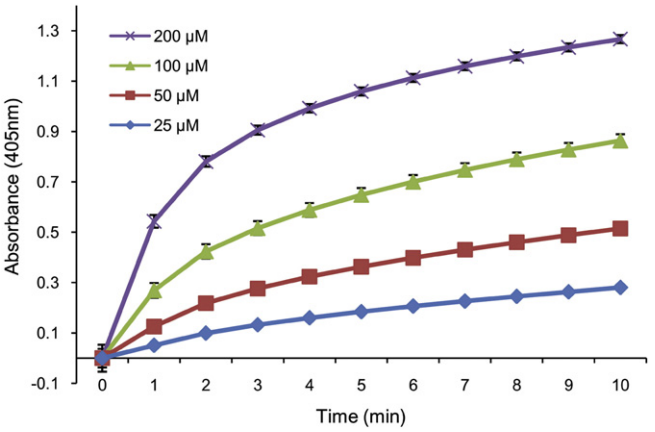

Figure 1. The concentration dependence of phosphate ester bond hydrolysis of pNPP by CNPs. The CNP concentration ranged from 25 μM to 200 μM. Experiments were performed in triplicate, and a representative experiment is shown.

Results

CNPs as a phosphatase mimetic

The reaction of CNPs with pNPP occurs readily at room temperature and neutral pH in a concentration-dependent manner as shown in Figure 1. The activity of CNP hydrolysis of the pNPP phosphate ester bond at pH 7 is calculated to be 0.860 ± 0.010 nmol *p*-nitrophenol/min/μg CNPs (200 μM) at 10 minutes. To determine the effect of pH on the hydrolysis, we performed the reaction of pNPP and CNPs (100 μM) at pH 4, pH 7, and pH 10. We compared the initial slopes of the plots of *p*-nitrophenol concentration at different pH values as a function of time and determined that the initial relative rate of the reaction is 1.7 times faster at pH 4 than at pH 7. Results indicate that at pH 10, the

Table 1
Comparison of the relative initial rates of phosphate ester bond hydrolysis of pNPP by CNPs (100 μM) at different pH values

pH value	Relative rate of reaction*
4	1.7
7	1
10	0.1

* The reaction rates are relative to the rate at pH 7. The data presented are an average of triplicate experiments. The standard deviation is less than 5%.

initial relative rate of the reaction is one-tenth of the rate at pH 7 (see Table 1). The hydrolysis of phosphate esters can depend on pH and exhibit slower rates at higher pH due to different reaction pathways[25] or possibly to changes in the surface charge of the nanoparticles at high pH.[26]

Oxidation state dependence

Single molecular complexes of $Ce_{(IV)}$ have been shown to be effective at cleaving the phosphate ester bond in solution.[14,27] $Ce_{(III)}$ complexes participating in DNA hydrolysis contain $Ce_{(IV)}$ active species.[28] Because CNPs possess mixed valence states of cerium, $Ce_{(III)}$ and $Ce_{(IV)}$, we determined the effect of oxidation state on phosphate ester bond hydrolysis. We have previously shown by XPS that hydrogen peroxide is effective at converting $Ce_{(III)}$ to $Ce_{(IV)}$ in CNPs.[29] The CNPs (100 μM) were pretreated with 3% hydrogen peroxide. The CNPs changed color from light yellow to orange after peroxide treatment. The CNPs were washed with water before the addition of pNPP to rinse away residual peroxide. Results show that the reaction depends on $Ce_{(III)}$ sites, and that the activity of hydrogen peroxide–pretreated CNPs is approximately 40% of the untreated CNPs (Figure 2). These results indicate that $Ce_{(III)}$ sites are the more active site in the hydrolysis reaction. An important consideration is that the hydrogen peroxide may alter the surface chemistry of the nanoparticle; however, hydrogen peroxide is effective in converting $Ce_{(III)}$ to $Ce_{(IV)}$ as is demonstrated by the XPS and absorbance data, and thus reduces catalytic activity of CNPs.

Free-phosphate ion production

We monitored the amount of free phosphate produced in the phosphate ester bond cleavage, and this method enabled us to determine the reactivity of CNPs toward other biologically relevant molecules such as ATP and *o*-phospho-L-tyrosine, whose cleavage products would not be as readily monitored via ultraviolet-visible spectroscopy. The amount of free phosphate was determined using a malachite green assay. In the first set of experiments we investigated the hydrolysis reaction of pNPP. The amount of free phosphate produced is dependent on the amount of CNPs added, and the amount of phosphate produced is approximately 4 nmol at the highest concentration of CNPs used (0.24 mM). Results show that the amount of free phosphate is relatively unchanged whether the reaction time is 1 hour or 4 hours, and the amount of phosphate produced depends on the concentration of CNPs (Figure 3, *A*). At the highest concentration of CNPs, there is no increase in free phosphate from 1 hour to 4 hours, indicating that the reaction has reached completion by 1 hour. These data indicate a

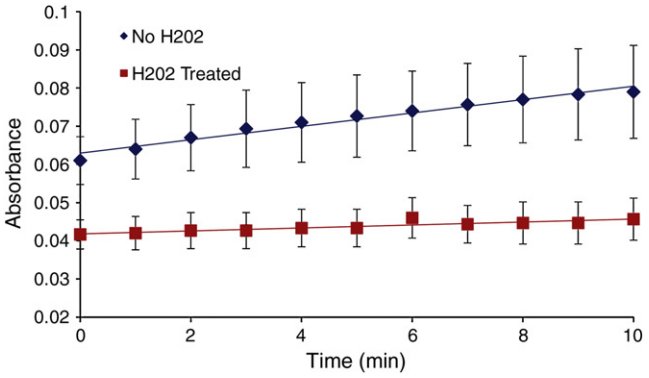

Figure 2. Comparison of CNP hydrolysis of pNPP after hydrogen peroxide pretreatment to untreated CNPs. Experiments were performed in triplicate, and a representative experiment is shown.

potential interaction of CNPs with phosphorylated proteins and molecules present in the cell, an important finding in light of the potential therapeutic applications of CNPs.

In the next set of experiments, we monitored the amount of free phosphate produced in the reaction of CNPs with ATP and *o*-phospho-L-tyrosine. Using ATP as the substrate at room temperature, the amount of free phosphate produced (CNPs = 0.24 mM) is approximately 3.0 nmol at 4 hours (data not shown). At 6 hours, the amount of free phosphate reaches 3.4 nmol (Figure 3, *B*). Additionally, the phosphate ester bond of *o*-phospho-L-tyrosine is hydrolyzed by CNPs; however, this reaction must be performed at 37°C. At 4 hours, 0.8 nmol of free phosphate is produced (Figure 3, *C*). These results indicate that CNPs can potentially react with ATP and phosphorylated proteins inside a cell. Although the hydrolysis of ATP and *o*-phospho-L-tyrosine do not occur as readily as with pNPP, the bond cleavage does occur under physiologically relevant conditions.

CNPs interaction with DNA

To investigate the interaction of CNPs with DNA, we added a solution of a known concentration of a DNA plasmid to CNPs. The CNPs removed the DNA plasmid from solution, suggesting concentration dependence on CNPs (Figure 3, *D*). Smaller fragments of DNA were not seen on the gel, indicating that the CNPs had not cut the DNA. CNPs interact with DNA by binding DNA rather than hydrolysis of the phosphate ester bond. We also monitored the free-phosphate concentration on samples of DNA plasmid incubated with a range of CNP concentrations (25 mM to 40 mM) at both room temperature and 37°C to verify that the phosphate backbone was still intact. We found that the free-phosphate levels of the DNA with CNPs were not above the DNA-only samples (no CNPs) at room temperature and at 37°C, providing additional support that the DNA remains intact.

Computational study of the dephosphorylation mechanism

A nanoparticle of 3 nm in diameter contains thousands of atoms and is too large a system to study with the first-principles simulations. Therefore, a representative fragment must be selected for the detailed study. Here we assume the surface of CNPs is

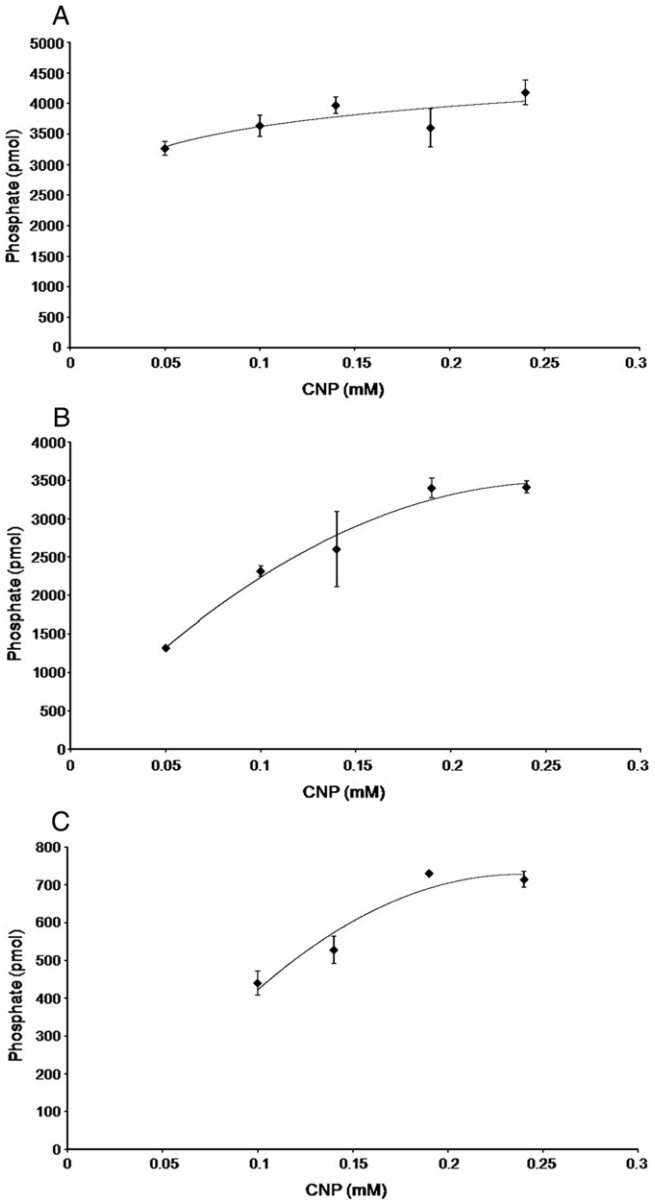

Figure 3. Comparison of the free-phosphate production from hydrolysis of **(A)** pNPP (4 hours at 25°C), **(B)** ATP (6 hours at 25°C), and **(C)** *o*-phospho-L-tyrosine (4 hours at 37°C) using the malachite green assay. Experiments were performed in triplicate, and a representative experiment is shown. **(D)** DNA gel electrophoresis data. Various concentrations of CNPs were incubated with mTERT plasmid at 37°C. After centrifugation, the supernatant was loaded on the gel. The DNA is removed from solution in a CNP concentration–dependent manner. No cleavage products are detected on the gel, nor are free-phosphate groups detected via the malachite green assay.

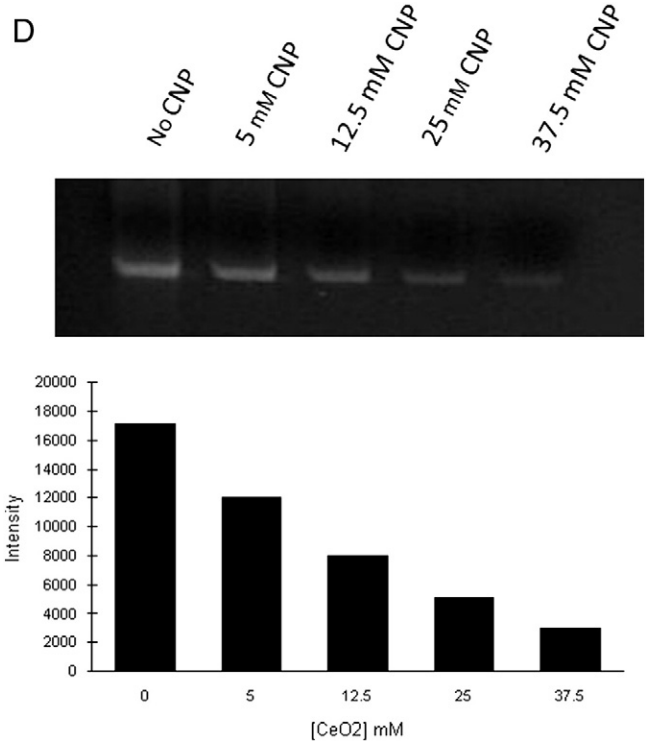

Figure 3 (continued).

mostly formed by oxygen-terminated (111) crystallographic planes. The ideal surface consists of hexagonal close-packed planes of oxygen ions and an underlying hexagonal close-packed plane of cerium ions. The triangular sites formed by the oxygen ions above the cerium ions present Lewis acidic centers and can be occupied by water molecules, phosphate ions, or other nucleophiles present in an aqueous environment. Additional acidic centers present are the oxygen vacancies, and these are also likely to be filled with nucleophiles. These nucleophiles complete the coordination sphere of the cerium ions to cubic (eight ligands), typical for $Ce_{(IV)}$ and $Ce_{(III)}$. The surface oxygen ions of the top layer serve as the bridging ligands for the three cerium ions from the layer below and probably exchange protons with the water molecules that occupy the triangular holes over the cerium ions. We will further assume that phosphate anion occupies two triangular holes, replacing two water molecules to coordinate to two cerium ions.

Based on the surface structure described above, we selected a hydroxo complex with two cerium ions, coordinated with eight hydroxide ligands each (two of them are μ-bridging the cations), and one bridging phosphate as a representative fragment of this surface (Figure 4, *A*) to describe the mechanism for the hydrolysis of the phosphate ester bond. To preserve the electroneutrality of the system, several hydroxide ligands were protonated. Next, we located the transition state containing a trigonal bipyramidal phosphorus atom with an additional hydroxide attached to it and followed the intrinsic reaction coordinate downhill on both the reactant and product sides. Several snapshots of the reaction pathway are shown in Figure 4. As shown, the neutral water molecule from the secondary coordination sphere (Figure 4, *A*) first switches its hydrogen bonding to the bridging hydroxide anion (Figure 4, *B*), and then transfers the proton along this newly formed hydrogen bond (Figure 4, *C*). The uncoordinated hydroxide that is formed then attacks pNPP (Figure 4, *D*) and forms the transition state (Figure 4, *E*). Next, the pNPP anion leaves (Figure 4, *F*), deprotonates one of the water molecules in the first coordination sphere (Figure 4, *G*), and forms the hydrogen-bonded product complex in the secondary coordination sphere (Figure 4, *H*).

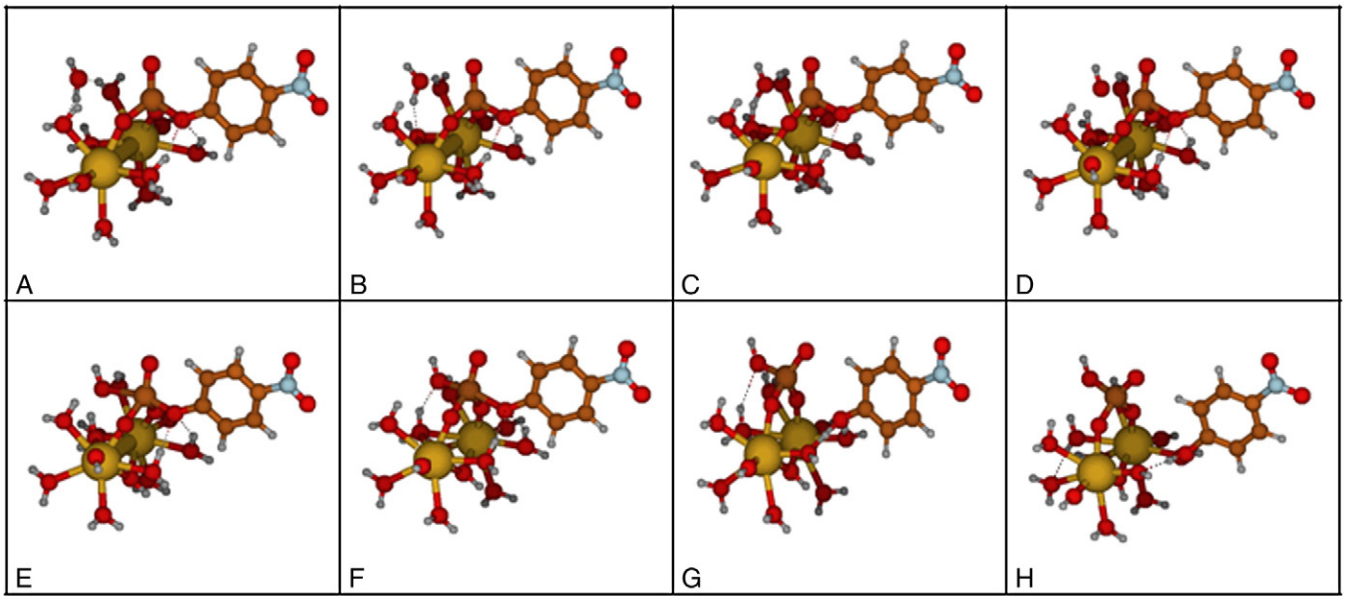

Figure 4. The snapshots of the reaction pathway for pNPP hydrolysis catalyzed by CNPs. **(A)** The reaction complex includes the neutral water molecule in the secondary coordination sphere. **(B)** The hydrogen bonding is switched to the bridging hydroxide anion. **(C)** The proton is transferred along this newly formed hydrogen bond. **(D)** The formed uncoordinated hydroxide then attacks pNPP and **(E)** forms the transition state. **(F)** The *p*-nitrophenyl anion then leaves, **(G)** deprotonates one of the water molecules in the first coordination sphere, and **(H)** forms the hydrogen-bonded product complex.

The difference in energy between the transition state (Figure 4, *D*) and reactant complex (Figure 4, *A*) determines the activation energy of the rate-determining step. This energy was calculated at UBMK/6-31G*/PCM theory level to be 22.9 kcal/mol for the $Ce_{(IV)}$-$Ce_{(IV)}$ complex, 16.0 kcal/mol for the $Ce_{(IV)}$-$Ce_{(III)}$ complex, and 13.6 kcal/mol for the $Ce_{(III)}$-$Ce_{(III)}$ complex. Successive reduction of the cerium ions lowers the calculated activation energy considerably (by ~5 kcal/mol) due to the relative stabilization of the transition state. Based on the Mulliken charges (not shown), we attribute this stabilization to the less polarized (more covalent) phosphorus-oxygen bonds in the phosphate-$Ce_{(III)}$-$Ce_{(III)}$ complex. Therefore, the origin of superior catalytic effect of the $Ce_{(III)}$ over $Ce_{(IV)}$ is purely electronic, and substantial geometrical differences need not be involved. Thus, our experimentally observed decrease in the hydrolysis rate catalyzed by peroxide-treated CNPs finds an explanation based on the simulation results.

Discussion

In this report the reactivity of CNPs toward phosphate ester bonds of biologically relevant molecules was investigated. CNPs have garnered considerable interest recently because of their potential applications as therapeutics and their free radical–scavenging capability, which stems from their ability to cycle between Ce^{4+} and Ce^{3+}. If CNPs are to be utilized as therapeutics, the interactions of these nanoparticles with biological molecules must be understood. Phosphorylated molecules are ubiquitous in a biological system, participate in protein regulation and energy transfer, and are an essential part of the structure of DNA.

The CNPs utilized for this study are 3–5 nm in size. CNPs of this size demonstrate free radical–scavenging capability, low toxicity, and ability to confer protection against radiation damage both in vitro and in vivo.[2] The results of this study demonstrate that CNPs cleave the phosphate ester bonds in pNPP, ATP, and *o*-phospho-L-tyrosine. The dephosphorylation reaction depends on the presence of Ce^{3+} sites and is inhibited when Ce^{3+} is converted to Ce^{4+}. Interestingly, CNPs do not dephosphorylate DNA. These findings are consistent with the use of CNPs as transfection reagents[30] and suggest that DNA may interact with CNPs, in a similar manner as DNA with the nucleosome, by wrapping around the nanoparticle.[31]

Computational modeling was employed to better understand the mechanism of dephosphorylation by CNPs. The transition state for the phosphate hydrolysis is very similar to the one established for the nucleophilic substitution at the aliphatic carbon atom (the S_N2 mechanism). Our conclusions about pNPP hydrolysis can be extended to the hydrolysis of the terminal phosphate group in ATP and *o*-phospho-L-tyrosine. Unlike pNPP with one ester oxygen atom, the phosphate groups in DNA have two ester links, whereas two remaining oxygen atoms of the phosphate coordinate to two cerium ions on the CNP surface. Apparently, in this system the phosphorus atom is too sterically hindered to undergo the nucleophilic substitution, similar to the tertiary carbon atom, which is inactive in the S_N2 mechanism, thus explaining the catalytic inactivity of CNPs toward DNA hydrolysis. On the other hand, single nuclear $Ce_{(IV)}$ complexes leave one oxygen atom of the phosphate uncoordinated, and DNA hydrolysis takes place.

Results from the computational study of the mechanism of dephosphorylation indicate that the surface hydroxyl groups on the nanoparticle must be protonated. This result is consistent

with the experimental findings that the dephosphorylation of pNPP proceeds faster at pH 4 and more slowly at pH 10. The activation energy for dephosphorylation is lower for the $Ce_{(III)}$-$Ce_{(III)}$ center than for either the $Ce_{(IV)}$-$Ce_{(III)}$ center or the $Ce_{(IV)}$-$Ce_{(IV)}$ center, which is in agreement with the finding that dephosphorylation is inhibited when cerium is in the +4 oxidation state. This finding is interesting, because single nuclear complexes of cerium that cleave phosphate ester bonds tend to be $Ce_{(IV)}$, not $Ce_{(III)}$ as is the case with CNPs.

These studies characterize for the first time to our knowledge the reactivity of CNPs toward phosphate ester bonds of biologically relevant molecules. These reactions are shown to occur readily at physiological pH. This reactivity may be an important consideration when designing and utilizing CNP therapeutics. Additional studies on the mechanisms and pathways that CNPs affect in biological systems are currently being investigated in our laboratory.

Acknowledgments

M.H.K. would like to thank Aaron Muth and Christophe Brandily of the University of Central Florida for their help with nuclear magnetic resonance spectroscopy.

Appendix A. Supplementary data

Supplementary data associated with this article can be found, in the online version, at doi:10.1016/j.nano.2010.05.004.

References

1. Tarnuzzer RW, Colon J, Patil S, Seal S. Vacancy engineered ceria nanostructures for protection from radiation-induced cellular damage. Nano Lett 2005;5:2573-7.
2. Colon J, Herrera L, Smith J, Patil S, Komanski C, Kupelian P, et al. Protection of radiation-induced pneumonitis using cerium oxide nanoparticles. Nanomed Nanotechnol Biol Med 2009;5:225-31.
3. Schubert D, Dargusch R, Raitano J, Chan SW. Cerium and yttrium oxide nanoparticles are neuroprotective. Biochem Biophys Res Commun 2006;342:86-91.
4. Silva GA. Seeing the benefit of ceria. Nat Nanotechnol 2006;1:92-4.
5. Rawlings J, Cleland WW, Hengge AC. Metal ion catalyzed hydrolysis of ethyl *p*-nitrophenyl phosphate. J Inorg Biochem 2003;93:61-5.
6. Franklin SJ. Lanthanide-mediated DNA hydrolysis. Curr Opin Chem Biol 2001;5:201-8.
7. Branum ME, Que Jr L. Double-strand DNA hydrolysis by dilanthanide complexes. J Biol Inorg Chem 1999;4:593-600.
8. Branum ME, Tipton AK, Zhu S, Que Jr L. Double-strand hydrolysis of plasmid DNA by dicerium complexes at 37 degrees C. J Am Chem Soc 2001;123:1898-904.
9. Katada H, Seino H, Mizobe Y, Sumaoka J, Komiyama M. Crystal structure of Ce(IV)/dipicolinate complex as a catalyst for DNA hydrolysis. J Biol Inorg Chem 2008;13:249-55.
10. Bunn SE, Liu CT, Lu ZL, Neverov AA, Brown RS. The dinuclear Zn(II) complex catalyzed cyclization of a series of 2-hydroxypropyl aryl phosphate RNA models: progressive change in mechanism from rate-limiting P-O bond cleavage to substrate binding. J Am Chem Soc 2007;129:16238-48.
11. Cassano AG, Anderson VE, Harris ME. Understanding the transition states of phosphodiester bond cleavage: insights from heavy atom isotope effects. Biopolymers 2004;73:110-29.
12. Livieri M, Mancin F, Sailelli G, Chin J, Tonellato U. Mimicking enzymes: cooperation between organic functional groups and metal ions in the cleavage of phosphate diesters. Chemistry 2007;13:2246-56.
13. Komiyama M, Takeda N, Shigekawa H. Hydrolysis of DNA and RNA by lanthanide ions: mechanistic studies leading to new applications. Chem Commun 1999:1443-51.
14. Sumaoka J, Furuki K, Kojima Y, Shibata M, Hirao K, Takeda N, et al. Active species for Ce(IV)-induced hydrolysis of phosphodiester linkage in cAMP and DNA. Nucleosides Nucleotides Nucleic Acids 2006;25:523-38.
15. Tan F, Zhang Y, Wang J, Wei J, Cai Y, Qian X. An efficient method for dephosphorylation of phosphopeptides by cerium oxide. J Mass Spectrom 2008;43:628-32.
16. Tomalia DA. In quest of a systematic framework for unifying and defining nanoscience. J Nanoparticle Res 2009;11:1251-310.
17. Korsvik C, Patil S, Seal S, Self W. Superoxide dismutase mimetic properties exhibited by vacancy engineered ceria nanoparticles. Chem Commun 2007:1056-8.
18. Frey ST, Hutchins BM, Anderson BJ, Schreiber TK, Hagerman ME. Catalytic hydrolysis of 4-nitrophenyl phosphate by lanthanum(III)-hectorite. Langmuir 2003;19:2188-92.
19. Frisch MJ, Trucks GW, Schlegel HB, Scuseria GE, Robb MA, Cheeseman JR, et al. Gaussian 03. Revision D.1. Wallingford, CT: Gaussian, Inc; 2004.
20. Schaftenaar G, Noordik JH. Molden: a pre- and post-processing program for molecular and electronic structures. J Computer-Aided Mol Design 2000;14:123-34.
21. Cundari TR, Stevens WJ. Effective core potential methods for the lanthanides. J Chem Phys 1993;98:5555-65.
22. Boese AD, Martin JML. Development of density functionals for thermochemical kinetics. J Chem Phys 2004;121:3405-16.
23. Peng CY, Ayala PY, Schlegel HB, Frisch MJ. Using redundant internal coordinates to optimize equilibrium geometries and transition states. J Comput Chem 1996;17:49-56.
24. Dinescu A, Clark AE. Thermodynamic and structural features of aqueous Ce(III). J Phys Chem A 2008;112:11198-206.
25. Morrow JR, Trogler WC. Hydrolysis of phosphate diesters with copper (II) catalysts. Inorg Chem 1988;27:3387-94.
26. Patil S, Sandberg A, Heckert E, Self W, Seal S. Protein adsorption and cellular uptake of cerium oxide nanoparticles as a function of zeta potential. Biomaterials 2007;28:4600-7.
27. Ott R, Kramer R. DNA hydrolysis by inorganic catalysts. Appl Microbiol Biotechnol 1999;52:761-7.
28. Komiyama M, Kodama T, Takeda N, Sumaoka J, Shiiba T, Matsumoto Y, et al. Catalytically active species for $CeCl_3$-induced DNA hydrolysis. J Biochem 1994;115:809-10.
29. Heckert EG, Karakoti AS, Seal S, Self WT. The role of cerium redox state in the SOD mimetic activity of nanoceria. Biomaterials 2008;29:2705-9.
30. Link N, Brunner TJ, Dreesen IAJ, Stark WJ, Fussenegger M. Inorganic nanoparticles for transfection of mammalian cells and removal of viruses from solution. Biotechnol Bioeng 2007;98:1083-93.
31. Berg MA, Coleman RS, Murphy CJ. Nanoscale structure and dynamics of DNA. Phys Chem Chem Phys 2008;10:1229-42.